Invited Paper

The Rationality of 2-D Simplification of Low-Speed Short Microchannel Flows*

Zuu-Chang Hong**,1, Ying-Jhe Pan[1], Yu-Chung Chiu[1] and Chien-Yuh Yang[2]

[1]*Department of Mechanical and Electro-Mechanical Engineering, Tamkang University*
151 Ying-Chuan Road, Tamsui, Taipei County 251, Taiwan, R.O.C.
[2]*Department of Mechanical Engineering, National Central University*
300 Jhongda Road, Jhongli City, Tayuan County 32001, Taiwan, R.O.C.

ABSTRACT

The Direct-simulation Monte Carlo (DSMC) method has been employed to analyze the rationality of the 2-D simplification for a 3-D straight rectangular cross-sectional channel, a 3-D straight rectangular cross-sectional channel with microstructures and a 3-D straight rectangular cross-sectional channel with a backward-facing step. An implicit treatment for low-speed inflow and outflow boundaries for the DSMC of the microchannel flow is employed. The 3-D microchannel flows are simulated with the various cross-aspect ratios ranging between 1 and 5. The calculated heat and flow properties in the 3-D cases are compared with the results of the 2-D case. It shows that when the aspect ratio is less than 3, the two extra side walls in the 3-D case have significant effects on the heat transfer and flow properties. When the aspect ratio increases, the flow properties and heat transfer characteristics of the 3-D simulations tend to approach that of the 2-D results. This paper also provides the information of the approaching level for different geometry of the microchannels. It is found that the approaching level becomes slower when the geometry of the channel becomes more complicated. In the present study , when the cross-section aspect ratio is 5 , the approaching level of the above mentioned three different geometry of microchannels are found to be about 99%, 97.8% and 97% respectively.

Keywords: DSMC, 3-D microchannel, Low-speed flow

I. INTRODUCTION

Since the significant applications of Micro-electro-mechanical system (MEMS) in medical and engineering problems, the understanding of the flow and heat transfer characteristics of the micro devices is important. The most essential elements of MEMS are the microchannels. In order to design and fabricate microsystems successfully, a deeper understanding of the flow and heat transfer characteristics in the microchannels is required [1, 2].

In most microchannel systems, the characteristic length of the system becomes comparable with the mean free path of the gas molecules inside the microchannel. Under such situations, the Knudsen number, $Kn=\lambda/L$, where λ is the mean free path of the gas molecules and L is the characteristic length of the system, is in a rarefied gas flow regime ranging from 0.01 to 10. When the flows are in the rarefied gas flow regime, the Navier-Stokes equations approximation, which based on the assumption of continuum, becomes an improper approach. The flows are better described from the molecular point of view, as opposed to the continuum point of view. Applied traditional continuum based techniques to MEMS flow analyses may therefore lead to large errors in the predictions [3].

The Direct-simulation Monte Carlo (DSMC) method proposed by Bird in 1963 is a well-developed

* Manuscript received, Oct. 20, 2008, final revision, Jan. 19, 2009
** To whom correspondence should be addressed, E-mail: zchong@mail.tku.edu.tw

method for simulating gas flows in which Kn is larger than 0.1 [4]. The DSMC method simulates a gas flow by storing the velocities and positions of thousands or millions of simulated molecules in computers. And, each simulated molecules represents a large number of real gas molecules. The motions of the simulated molecules are deterministic but the intermolecular collisions and the interactions between the molecules and physical boundaries are processed by probabilistic method. The macroscopic flow quantities, such as velocity and temperature, are obtained via sampling the calculated molecular properties. In the beginning, the DSMC has usually been applied to study problems in rarefied gas flows, such as the rarefied free shear layer at hypersonic speed [5]. The DSMC computations of the high-speed, high-Knudsen-number flow in a microchannel can be found in [6-11]. Some good reviews can be found in Muntz [12] and Oran et al. [13].

Usually, the flow velocity in the microchannels used in MEMS is less than the speed of sound. Therefore, the typical stream and vacuum boundary conditions employed in DSMC calculations are not physically appropriate. Instead, the inflow and outflow conditions that impose the correct propagation of information across the boundaries must be applied to the low-speed microchannel flows. Nance, Hash and Hassan [14] have discussed the role of boundary conditions in the DSMC simulation of MEMS systems. Fan and Shen [15] have presented a DSMC-IP method which was a success for one-dimensional low-speed microchannel flows. Cai, Boyd and Fan [16] made some modifications to the DSMC-IP method and extended it to two-dimensional low-speed microchannel flows. Sun and Faghri [17] employed the DSMC method to investigate the effects of rarefaction and compressibility of gaseous flow in microchannel. Wu et al. [18] developed the particle-based boundary treatment to calculate a microchannel flow and a backward-facing micro-step gas flow. Fang and Liou [19] employed the DSMC method with implicit boundary conditions to calculate the heat transfer of the low-speed microchannel flows. Fang and Liou [20] calculated the heat transfer in microchannel flows and compared the results with the analytical solutions derived from the Navier-Stokes equations with slip-boundary conditions. Sun and Faghri [21] discussed the effect of surface roughness on nitrogen flow in a microchannel using the DSMC method. Wang and Li [22] developed the pressure boundary treatment according to the characteristics theory, which overcame the instability of particle-based boundary treatment. Wang and Li [23] employed the DSMC method with pressure boundary treatment to calculate the microchannel flow and discussed the three-dimensional effect of gas flow field in microchannels. Their study focused only on the flow field and the temperature field was not mentioned. Zhen et al. [24] employed the DSMC method with implicit boundary treatment to investigate the flow field and the heat transfer characteristics of a 3-D microchannel flows and compared to that of 2-D case. Hong et al. also investigated heat and fluid flow of 3-D microchannel with microstructures.[25] Xue et al. [26] employed the DSMC method to calculate micro backward-facing step flows and discussed the effects of rarefaction on flow characteristics. Wang and Li [27] investigated the mixing behavior of gas flows in microchannels using the DSMC method.

This paper employed the DSMC method with implicit boundary conditions reported in Liou and Fang [19] to calculate 3-D microchannel flows with different cross aspect ratios. This paper conferred with three kinds of 3-D straight rectangular cross-sectional channel flows, 3-D straight rectangular cross-sectional channel, 3-D straight rectangular cross-sectional channel with microstructures and 3-D straight rectangular cross-sectional channel with a backward-facing step. The heat transfer and flow properties of each 3-D case are calculated and compared to the results of the corresponding 2-D case. This paper discussed how the cross-section ratio and the geometry of the microchannel for the straight rectangular cross-sectional channel flows influence the rationality of the 2-D simplification.

II. NUMERICAL METHOD

2.1 Direct Simulation Monte Carlo Method

The DSMC method is a probabilistic simulation method that employs a large number of statistically selected simulated particles of the correct physical size. The position, velocities, and initial states of these simulated particles are stored and modified in every time-step, Δt, in the process of particles moving, colliding among themselves, and interacting with boundaries in the simulated physical space. Each particle represents a fixed number, F_n, of real particles. An important feature of the DSMC method is that the molecular motion and the intermolecular collisions are decoupled over time intervals, which are much smaller than the mean collision time.

The DSMC simulation algorithm is described in detail by Bird [4], and we give only a brief sketch here. Important steps of the DSMC method include setting up the initial conditions, moving all the simulated particles, indexing (or sorting) all the particles, colliding between particles, and sampling the molecules within cells to determine the macroscopic quantities.

The calculation zone is divided into computational cells, and each cell is also divided into subcells. The computational cells are used to facilitate the choice of molecules for collisions and for the sampling of the macroscopic flow properties such as pressure, density, and temperature. The time-step is set such that a typical molecule moves about one third of the cell dimension at each time-step [4]. In the current study, the variable hard sphere (VHS) model and the no time counter (NTC) method [4] are used to simulate the molecular collision kinetics. Energy exchange between kinetic and internal modes is controlled by the Larsen-Borgnakke statistical model [28].

2.2 Implicit Boundary Treatment

For flows at high speeds, such as hypersonic flows, the thermal velocity can be smaller in magnitude

compared with the mean velocity. For a DSMC simulation of high-speed flow, a conventional approach is to impose a "vacuum" condition at the exit boundary, where no molecules enter the computational domain from the region external to the flow domain. For the low-speed flows, the thermal motion can be of the same order of magnitude as the mean molecular motion. It then becomes inappropriate to neglect the mass influxes at a flow boundary.

The boundary treatment employed in this paper is proposed by Liou and Fang [19]. The derivation can also be found in Liou and Fang [19]. In this method, the number of molecules entering the computational domain and their corresponding internal energy and velocity components are determined in an implicit manner by the local mean flow velocity, temperature, and number density.

In order to implement the DSMC procedure, the number density, temperature and mean velocity at the flow boundaries are needed. At the upstream boundaries, the pressure, P_{in}, and density, ρ_{in}, are the given parameters of the flow. The number density, n_{in}, and temperature, T_{in}, can then be obtained according to the conservation of mass and the equation of state. That is,

$$n_{in} = \rho_{in} / m \tag{1}$$

$$T_{in} = p_{in} /(\rho_{in} R) \tag{2}$$

The transverse mean velocity, $(V_{in})_j$, is set to be zero. A first-order extrapolation is used to determine the inlet mean velocity, $(U_{in})_j$, from that of the computed velocity for cell j. That is,

$$\left(U_{in}\right)_j = U_j \tag{3}$$

At the downstream boundary, the only given flow parameter is the exit pressure, p_e. The other mean properties of the flow are to be determined as the calculation proceeds. In the present method, the flow variables are first computed by the following equations

$$(n_e)_j^k = n_j^k + \frac{p_e - p_j^k}{m(a_j^k)^2} \tag{4}$$

$$(u_e)_j^k = u_j^k + \frac{p_j^k - p_e}{m n_j^k a_j^k} \tag{5}$$

$$(v_e)_j^k = v_j^k \tag{6}$$

$$(w_e)_j^k = w_j^k \tag{7}$$

$$(T_e)_j^k = p_e /[(n_e)_j^k mR] \tag{8}$$

$$\left(U_e\right)_j = \frac{1}{N_j}\sum_{i=1}^{N_j} u_{e,i} \tag{9}$$

$$\left(V_e\right)_j = \frac{1}{N_j}\sum_{i=1}^{N_j} v_{e,i} \tag{10}$$

$$\left(W_e\right)_j = \frac{1}{N_j}\sum_{i=1}^{N_j} w_{e,i} \tag{11}$$

III. RESULTS AND DISCUSSION

The 3-D straight rectangular cross-section channel flows, the 3-D straight rectangular cross-section channel flows with microstructures and the 3-D straight rectangular cross-section channel flows with a backward-facing step are simulated with various cross aspect ratios and compared to the corresponding 2-D results. The gas inside the microchannel is assumed to be nitrogen and the characteristic-length is the height of the microchannel for the 3-D straight rectangular cross-section channel flows and the 3-D straight rectangular cross-section channel flows with microstructures. The characteristic-length is the height of the step for the 3-D straight rectangular cross-section channel flows with a backward-facing step. An implicit treatment proposed by Liou and Fang [19] for low-speed inflow and outflow boundaries for the DSMC of the microchannel flows is used. The variable hard sphere (VHS) model and diffusive wall boundary condition are used for the collision processes.

3.1 3-D Straight Rectangular Cross-sectional Channel Flows

The height of the microchannel, H, is 0.4μm, the length, L, is 2.0μm, and the width, D, is 0.4μm, 0.6μm, 1.2μm and 2.0μm for cases 1, 2, 3 and 4, respectively. In the 2-D case, the height, H, is 0.4μm, the length, L, is 2.0μm. Sketches of the simulated geometry are shown in Figure 1. The inlet flow temperature is 300 K, the inlet pressure is 2.5 atm, the pressure ratio (Pr) is 2.5 and the wall temperature is 323 K for both 3-D and 2-D cases. These operating conditions result in the values of the cross-section aspect ratio (cross-section aspect ratio = D/H) for the 3-D straight rectangular cross-sectional channel flow varies between 1 and 5 and the values of Knudsen number varies between 0.053 and 0.136. The aspect ratio is 1, 1.5, 3 and 5 in the cases 1, 2, 3 and 4, respectively. Due to the symmetry, only a quarter of the flow field is used in the simulation. Sketch of the computational domain is shown in Figure 2. In order to verify this symmetry assumption, a comparison between a quarter of the full domain and the full-domain is given in Figure 3. In order to save the simulation time, the height of the microchannel in full-domain case in figure 3 is 0.2μm, the length is 1.0μm, and the width is 0.2μm. The computational grid consists of 100×30×30, 100×45×30, 100×90×30, and 100×150×30 uniform rectangular cells in the cases 1, 2, 3 and 4, respectively. A constant velocity of 100 m/s is used uniformly in the computational domain to initiate the calculation. The number of simulated molecules is about 2,500,000, 2,500,000, 3,000,000 and 4,000,000 in cases 1, 2, 3 and 4,

respectively. The flow was run for 2000 time steps to allow any initial condition effect to die out, than sampled every two time step until 200,000 samples were reached. The calculations were carried out on Pentium 4 PCs. Cases 1 ,2 ,3 and 4 each takes about 200hr, 300hr, 600hr and 1000hr of CPU time, respectively.

The distributions of slip-velocity along the wall are shown in Figure 4. The slip-velocity is defined as

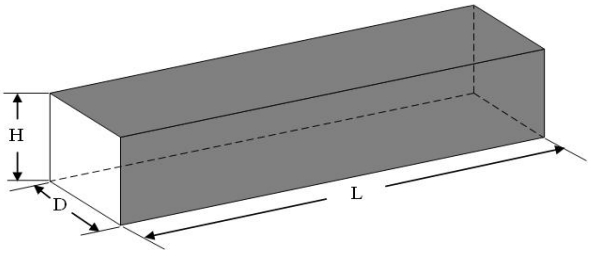

Figure 1 Sketch of the simulated geometry.

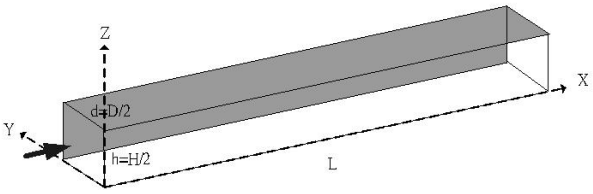

Figure 2 Sketch of the computational domain.

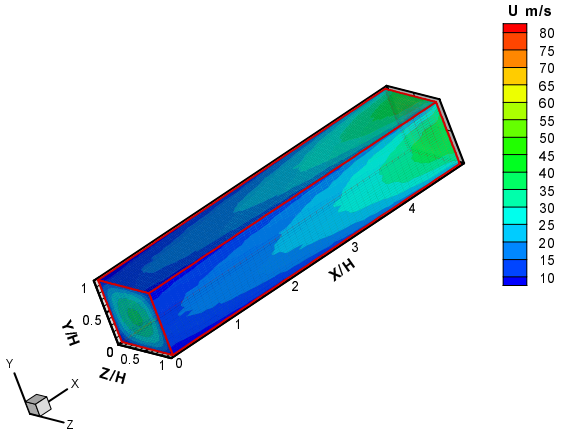

(a) Velocity profiles of full-domain case

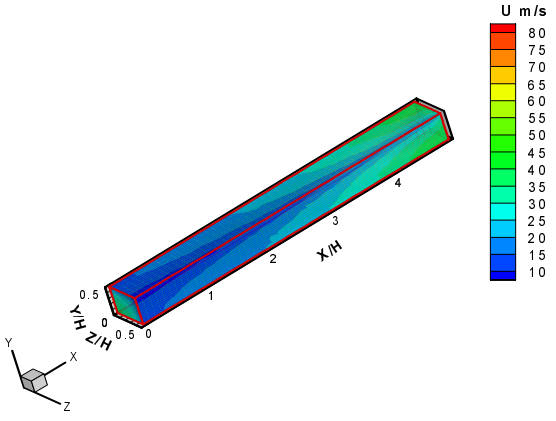

(b) Velocity profiles of a quarter of the domain case

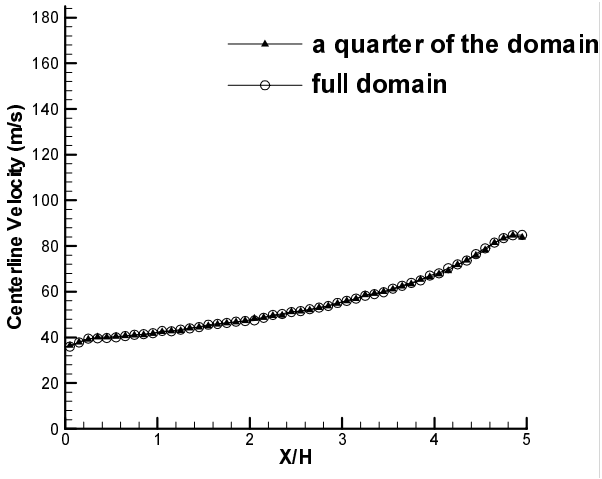

(c) Centerline velocity distributions

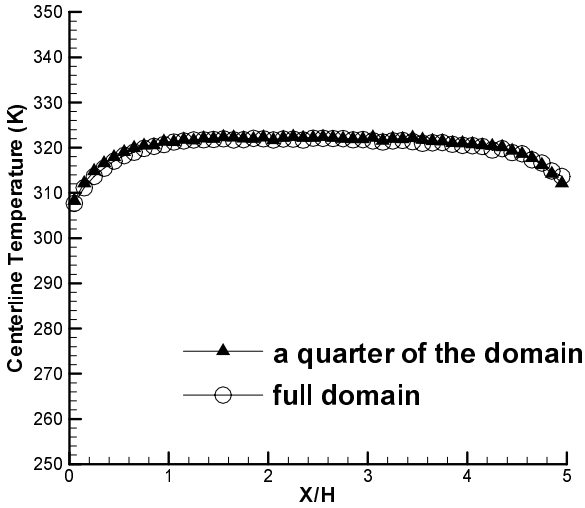

(d) Centerline temperature distributions

Figure 3 The comparison between a quarter of the domain computation and full-domain computation for (a) velocity profiles of full-domain case; (b) velocity profiles of a quarter of the domain case; (c) centerline velocity distributions; (d) centerline temperature distributions.

$$u_s = u_g - u_w \tag{12}$$

where u_g represents the gas velocity on a wall, and u_w the wall velocity. The distributions of the slip-velocity in case 1 and case 2 are obviously smaller than that in the 2-D case. This is due to the friction between the extra two side walls of the 3-D microchannel and the flow. The slip-velocity in case 1 is about 66% of that in the 2-D case. The slip-velocity in case 2 is about 83% of that in the 2-D case. The slip-velocity in case 3 is about 94% of that in the 2-D case. The slip-velocity in case 4 is about 99% of that in the 2-D case. As the value of the cross aspect ratio increases, the deviation of the slip-velocity between the 2-D case and the 3-D case decreases.

Figure 5 shows the distributions of the centerline velocity. The distributions of the centerline velocity in

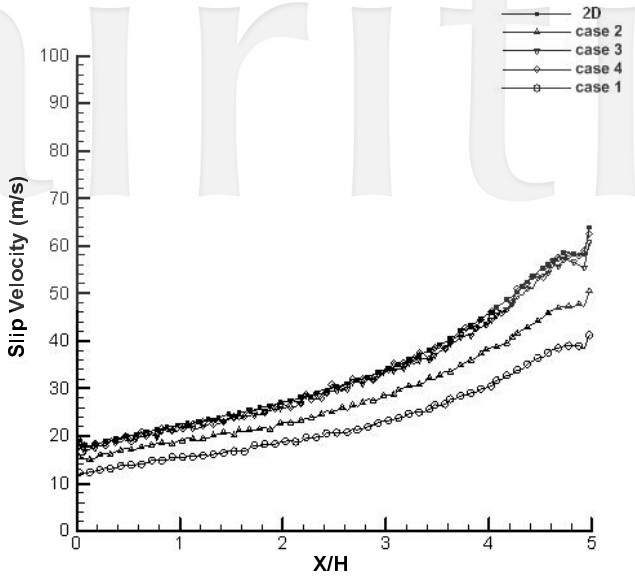

Figure 4 The distributions of slip-velocity along the wall.

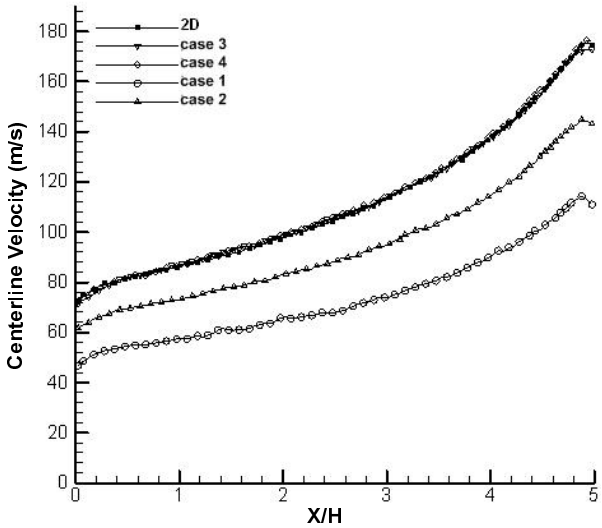

Figure 5 The distributions of the centerline velocity.

case 1 and case 2 are obviously smaller than that in the 2-D case. The centerline velocity in case 1 is about 65% of that in the 2-D case. The centerline velocity in case 2 is about 84% of that in the 2-D case. The centerline velocity in case 3 is about 99.99% of that in the 2-D case. The centerline velocity in case 4 is almost the same as case 3. As the value of the cross aspect ratio increases, the deviation of the centerline velocity between the 2-D case and the 3-D case decreases.

The distributions of the centerline temperature are shown in Figure 6. The centerline temperature in case 1 and case 2 is obviously higher than that in 2-D case. In case 1, the centerline temperature is about 4K higher than that in 2-D case at the location, X/H=2.5. In case 2, the centerline temperature is about 2K higher than that in 2-D case at the location, X/H=2.5. In case 3 and case 4, the deviation of the centerline temperature between the 3-D case and the 2-D case is less than 1K at the location, X/H=2.5. Figure 7 shows the distributions of the difference between the wall temperature and the gas temperature near the wall, or the temperature-jump. The temperature-jump is defined as

$$T_j = T_g - T_w \tag{13}$$

where T_g represents the gas temperature near the wall, and T_w is the wall temperature. As the value of the cross aspect ratio increases, the deviation of the temperature-jump between the 2-D case and the 3-D case decreases. In the entrance region, the temperature-jump in case 1 decreases very quickly. The results suggest that there are more collisions between the simulated molecules and the walls in case 1 than in the other cases due to the larger two side walls. Since there are more energy exchange between the simulated molecules and the walls, the temperature-jump in case 1 is smaller than that in the other cases. It can also be seen from Figure 8 which shows the distributions of the wall heat flux. To further illustrate the 3-D effect, the averaged (along y direction) heat flux distributions of each 3-D case and heat flux distribution of 2-D case are shown in Figure 9. Obviously, the cross aspect ratio is larger than 5, the results of 3-D calculations closely agree with those of 2-D calculations. The net heat flux on a wall element can be evaluated as

$$\dot{q} = \frac{\left[\sum_{i=1}^{n}\left(e_{tr,i}+e_{rot,i}\right)_{inc} - \sum_{i=1}^{n}\left(e_{tr,i}+e_{rot,i}\right)_{ref}\right]\cdot F_n}{t_s\left(\Delta y \cdot \Delta x\right)} \tag{14}$$

where n is the total number of simulated molecules that strike the wall element during sampling, F_n is the number of gaseous molecules associated with a simulated molecule, and t_s is the time period of the sampling. The

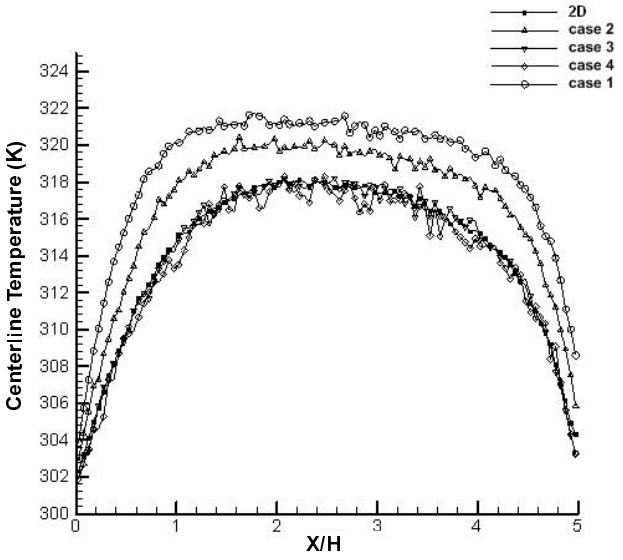

Figure 6 The distributions of the centerline temperature.

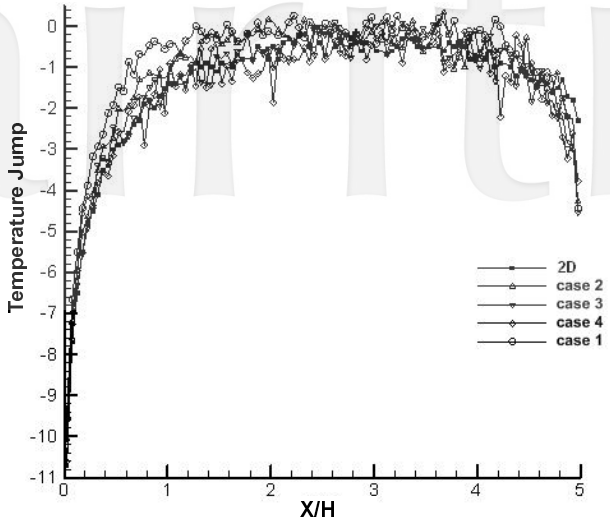

Figure 7 The distributions of the temperature-jump.

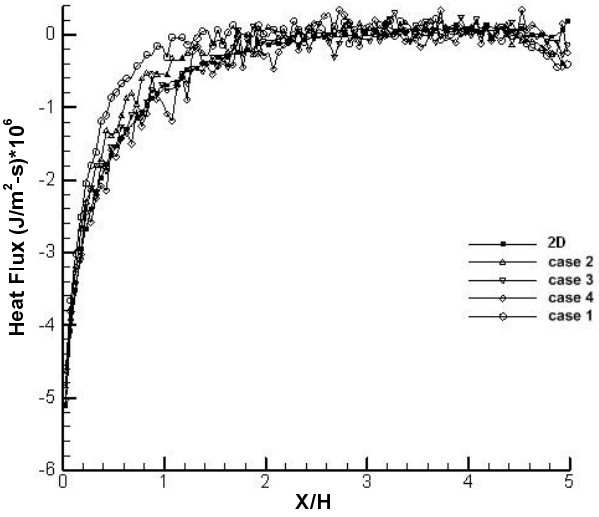

Figure 8 The distributions of the wall heat flux.

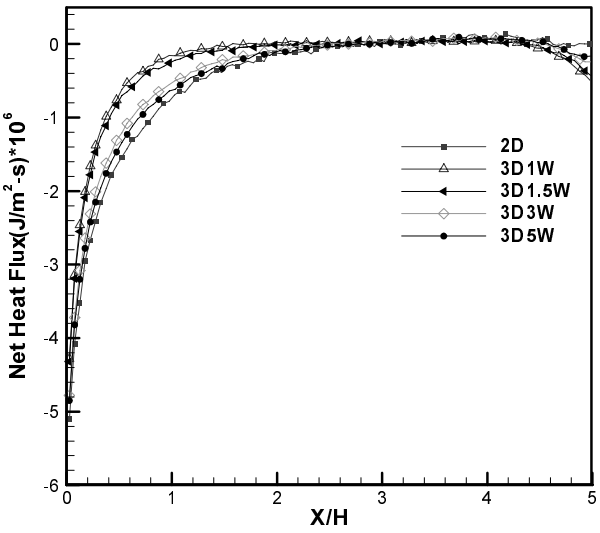

Figure 9 The averaged distributions of the wall heat flux.

subscripts "inc" and "ref" denote the values before and after the molecule impacts the wall, respectively. Since the value of the heat flux from the wall in case 1 is larger than that in other cases, the temperature-jump in case 1 is lower than that in other cases. As the value of the cross aspect ratio increases, the deviation of the wall heat transfer between the 2-D case and the 3-D case decreases. When the cross aspect ratio is larger than 5, the results of 3-D calculations are very close to that of 2-D calculation.

3.2 3-D Straight Rectangular Cross-sectional Channel Flows with Microstructures

The height of the microchannel, H, is 0.4μm, the length, L, is 2.0μm, and the width, D, is 0.4μm, 1.2μm and 2.0μm for cases 5, 6 and 7, respectively. The height of the microstructure is 0.2μm, the length is 0.332μm and the width is the same with the microchannel. The volume ratio of the microstructure to the microchannel is about 0.166 .The front surface of the microstructure near the inlet is at the location X/H=1.255. The rare surface of the microstructure near the outlet is at the location X/H=4.035. The volume ratio of the two microstuctures to the microchannel is about 0.1. The inlet flow temperature is 300 K, the inlet pressure is 0.73 atm, the pressure ratio is 2.5, the temperature of the top wall of the microstructure is 523 K, and the wall temperature is 323 K. These operating conditions result in the values of the cross-section aspect ratio (cross-section aspect ratio = D/H) for the 3-D straight rectangular cross-sectional channel flow ranging between 1 and 5. The aspect ratio is 1, 3 and 5 in cases 5, 6 and 7, respectively. Sketches of the simulated geometry are shown in Figure 10. Due to the symmetry, only half of the flow field is used in the simulation. The computational domain consists of 100×10×20, 100×30×20 and 100×50×20 uniform rectangular cells for cases 5, 6 and 7, respectively. A constant velocity of 100 m/s is used uniformly in the computational region to initiate the calculation. The number of simulated molecules is about 2,500,000, 3,000,000 and 4,000,000 in cases 5, 6 and 7, respectively. The flow was run for 2000 time steps to allow any initial condition effects to die out, than sampled every two time steps until 200,000 samples were reached. The calculations were carried out on Pentium 4 and Core(TM)2 PCs. Cases 5, 6 and 7 each takes about 63hr, 96hr and 134hr of CPU time, respectively.

Figure 12 shows the distributions of the centerline velocity. The distributions of the centerline velocity in case 5 are obviously smaller than that in the 2-D case. The centerline velocity in case 5 is about 78% of that in the 2-D case. The centerline velocity in case 6 is about 97% of that in the 2-D case. The centerline velocity in case 7 is about 97.8% of that in the 2-D case. As the value of the cross aspect ratio increases, the deviation of the centerline velocity between the 2-D case and the 3-D case decreases.

The streamwise variations in temperature at two height levels for 2-D and 3-D cases are shown in Figures 13 and 14. One at the top of the microstructure is shown in Figure 13 and the other at midway between the top of the microstructure and the top wall is shown in Figure 14.

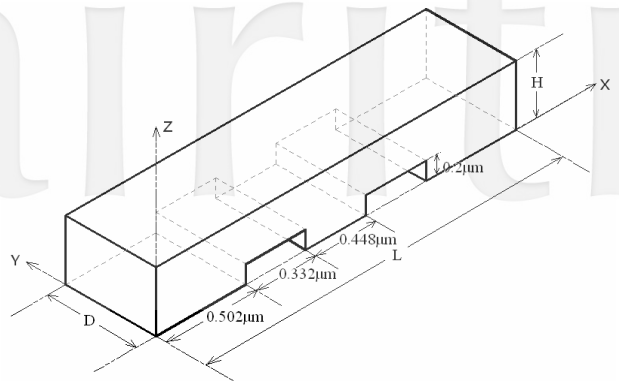

Figure 10 Sketch of the microchannel with microstructure.

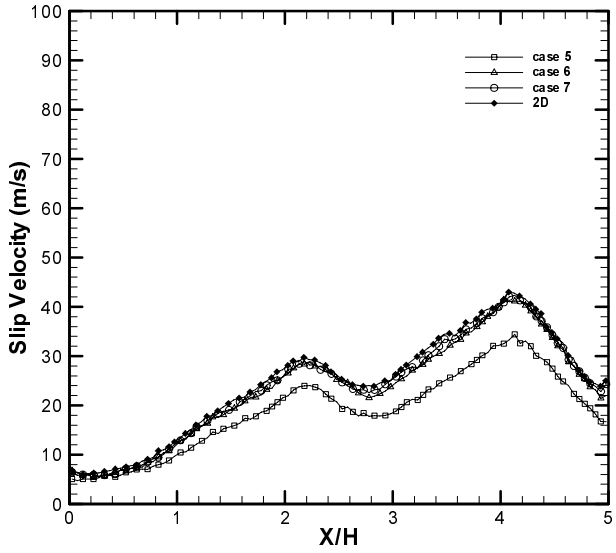

Figure 11 The distributions of slip-velocity along the wall.

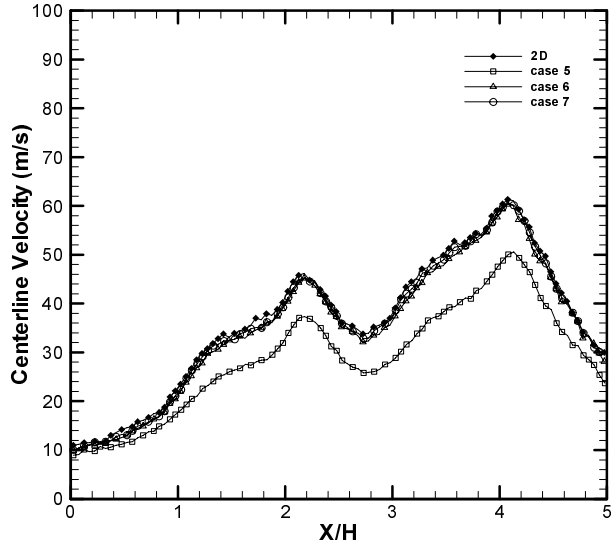

Figure 12 The distributions of centerline velocity.

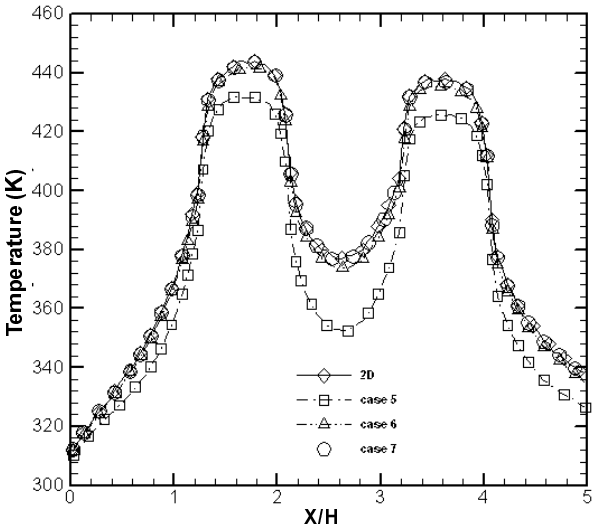

Figure 13 The distributions of temperature.

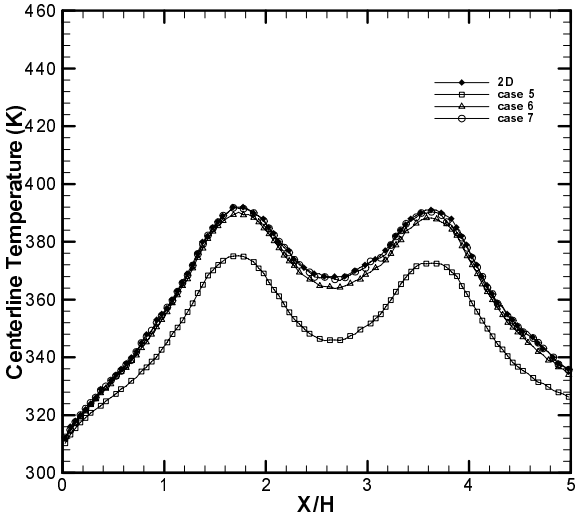

Figure 14 The distributions of centerline temperature.

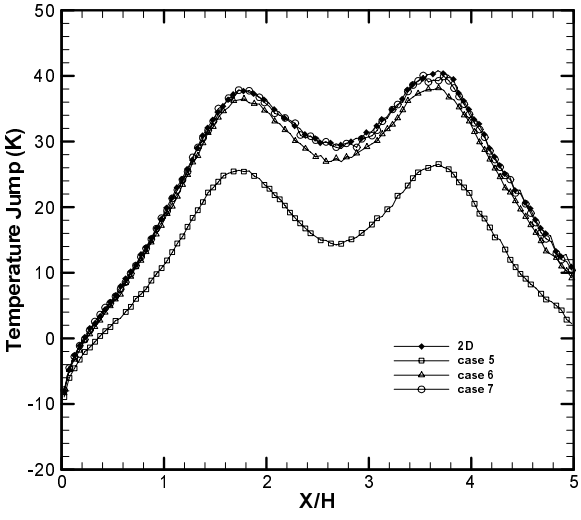

Figure 15 The distributions of the temperature-jump.

The temperature at the top of the microstructure in case 5 is obviously lower than that in the 2-D case. The temperature of case 5 is about 12 K lower than that in the 2-D case at the location, X/H=1.7. In cases 6 and 7, the deviation of temperature between the 3-D cases and the 2-D case is less than 2K and less than 1K at the location, X/H=1.7. The temperature at midway between the top of the microstructure and the top wall for case 5 in Figure 14 is obviously lower than that in the 2-D case. In case 5, the temperature is about 17 K lower than that in the 2-D case at the location, X/H=1.7. In cases 6 and 7, the deviation of centerline temperature between the 3-D cases and the 2-D case is less than 2K and less than 1K at the location, X/H=1.7.

As the value of the cross aspect ratio increases, the deviation of the centerline velocity and centerline temperature between the 2-D case and the 3-D case decreases. When the cross aspect ratio is larger than 5, the results of 3-D results are very close to that of 2-D result.

3.3 3-D Straight Rectangular Cross-sectional Channel Flows with a Backward-facing Step

The height of the microchannel, *H*, is 0.4μm, the length, *L*, is 2.0μm, and the width, *D*, is 0.4μm, 1.2μm and 2.0μm for cases 8, 9 and 10, respectively. The height of the step, *S*, is 0.2μm and the length of the step is 0.6μm. The characteristic length is the height of the step, *S*. The volume ratio of the step to the microchannel is about 0.15.The inlet flow temperature is 300 K, the inlet pressure is 0.1 atm, the pressure ratio is 2, the temperature of the step and the wall of the channel is 323 K. These operating conditions result in the values of the cross-section aspect ratio (cross-section aspect ratio = *D/H*) for the 3-D straight rectangular cross-sectional channel flow with a backward-facing step ranging between 1 and 5. The cross aspect ratio is 1, 3 and 5 in cases 8, 9 and 10, respectively. Sketches of the simulated geometry are shown in Figure 16. Due to the geometric symmetry, only half of the flow field is simulated. The computational domain consists of 60×6×12, 60×18×12 and 60×30×12 uniform rectangular cells for cases 8, 9 and 10, respectively. A constant velocity of 100 m/s is used uniformly in the computational region to initiate the calculation. The number of simulated molecules is about 1,800,000, 2,400,000 and 3,000,000 in cases 8, 9 and 10, respectively. The flow was run for 2000 time steps to allow any initial condition effects to die out, than sampled every two time steps until 200,000 samples were reached. The calculations were carried out on Pentium 4 and Core(TM)2 PCs. Cases 8, 9 and 10 each takes about 4hr, 38hr and 48hr of CPU time, respectively.

Figure 18 shows the distributions of the centerline velocity at midway between the top of the step and the top wall. The distributions of the centerline velocity in case 8 are obviously smaller than that of the 2-D case. The centerline velocity in case 8 is about 67% of that in the 2-D case. The centerline velocity in case 9 is about 92% of that in the 2-D case. The centerline velocity in case 10 is about 97% of that in the 2-D case. As the value of the cross aspect ratio increases, the deviation of the

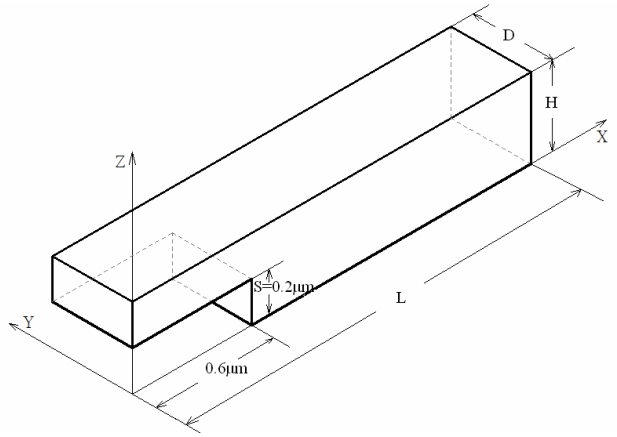

Figure 16 Sketch of the microchannel with step.

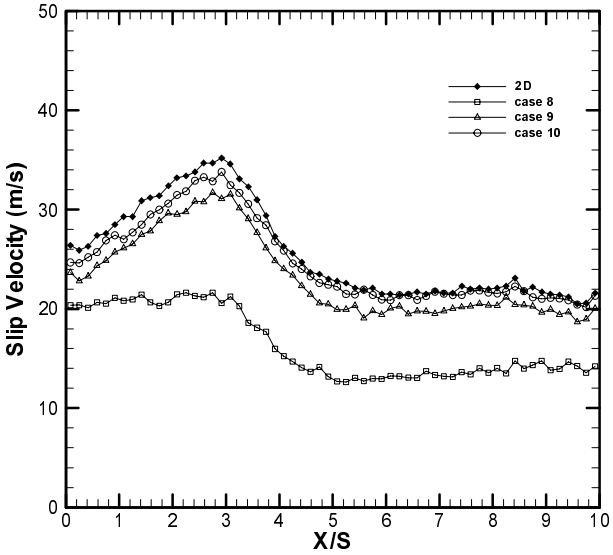

Figure 17 The distributions of slip-velocity along the wall.

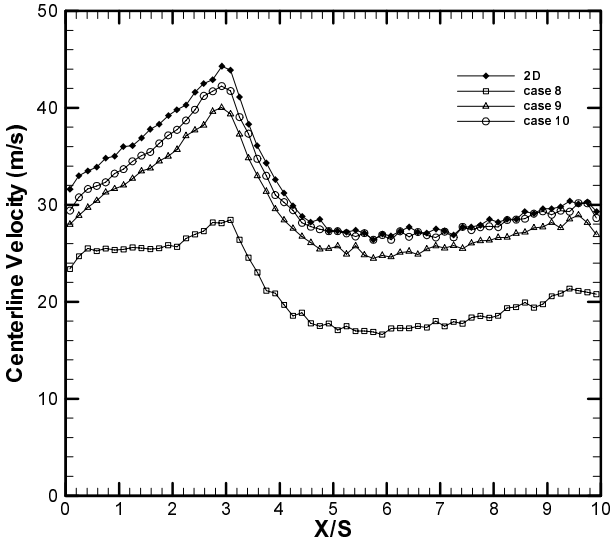

Figure 18 The distributions of centerline velocity.

centerline velocity between the 2-D case and the 3-D case decreases.

The streamwise variations in temperature at midway between the top of the step and the top wall for 2-D and 3-D cases are shown in Figures 19. The temperature at midway between the top of the step and the top wall in case 8 is obviously lower than that of the 2-D case. The temperature of case 8 is about 1K lower than that in the 2-D case at the location, X/S=10. In case 9, the temperature of case 9 is about 1K lower than that in the 2-D case at the location, X/S=10. In case 10, the deviation of temperature between the 3-D cases and the 2-D case is less than 1K at the location, X/S=10. As the value of the cross aspect ratio increases, the deviation of the centerline velocity and centerline temperature between the 2-D case and the 3-D case decreases. When the cross aspect ratio is larger than 5, the results of 3-D calculations are very close to that of 2-D calculation.

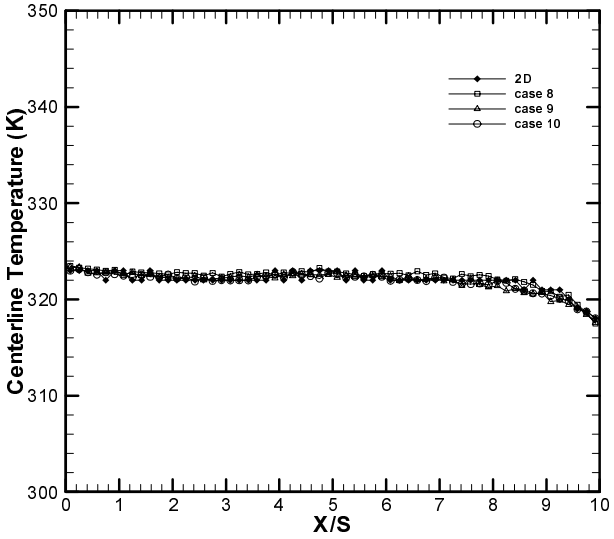

Figure 19 The distributions of the centerline temperature.

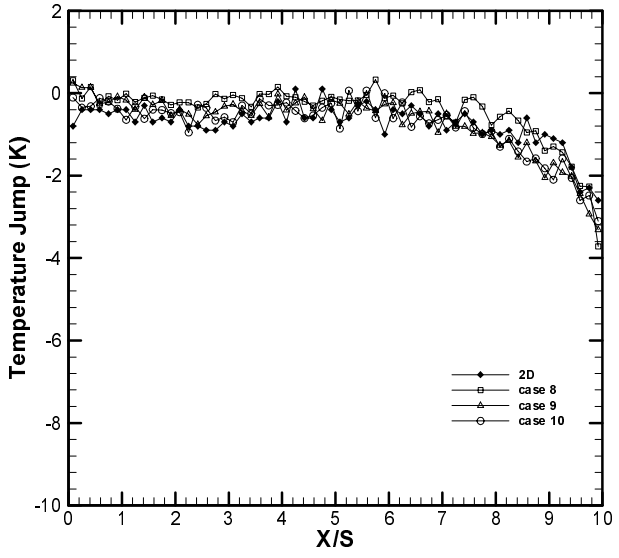

Figure 20 The distributions of the temperature-jump.

IV. CONCLUSIONS

The DSMC method is employed to simulate a 3-D straight rectangular cross-sectional channel, a 3-D straight rectangular cross-section channel with microstructures and a 3-D straight rectangular cross-section channel with a backward-facing step with various cross aspect ratios ranging between 1 and 5. An implicit treatment for low-speed inflow and outflow boundaries for DSMC is employed. The calculated results in the 3-D cases are compared with the results of the 2-D case. It shows that for all these three different geometry of microchannels, when the cross-section aspect ratio is less than 3, the side walls in the 3-D cases have significant effects on the heat transfer and flow properties. When the aspect ratio increases, the flow properties and heat transfer characteristics tend to approach that of the 2-D results. This paper also provides the information of the approaching levels for different geometry of the microchannels. These results are listed in table 1. It is found that the approaching level becomes slower when the geometry of the channel becomes more complicated. When the cross-section aspect ratio is 5, the approaching level of the above mentioned three different geometry of microchannels are found to be about 99%, 97.8% and 97% respectively.

NOMENCLATURE

a	speed of sound, m/s
D	channel width, m
e	energy, J
F_n	number of real molecules in DSMC simulation.
H	channel height, m
hr	hour
Kn	Knudsen number ($=\lambda/L$)
L	characteristic length, m
L	channel length, m
m	molecular mass, kg
N	number of sampling
n	number density, m^{-3}
P	pressure, Pa
$\dot{q}$	net heat flux, J/m^2s
R	gas constant, J/kg K
S	height of the step, μm
T	temperature, K
T_j	temperature jump, K
T_g	gas temperature, K
T_w	wall temperature, K
T_{block}	block temperature,K
T_{step}	step temperature,K
t_s	time period of the sampling, s
U, V, W	mean velocity components in x, y and z directions, m/s
u, v, w	molecular velocity components in x, y and z directions, m/s

Table 1.1 Simulation condition(cross-sectional channel)

CASE	1	2	3	4	2-D
Length(μ m)	2	2	2	2	2
Height(μ m)	0.2	0.2	0.2	0.2	0.4
Width(μ m)	0.2	0.3	0.6	1	
P_{in} (atm)	2.5				
P_{in}/P_e	2.5				
T_g (K)	300				
T_w (K)	323				
Number density	6.11×10^{25}				
Number of cells	100x30x30	100x45x30	100x90x30	100x150x30	100x60
Initial number of particles per cell	20				
CPU time	200 hr	300 hr	600 hr	1000 hr	12 hr
Computer rank equipment	P4 2.4 GHz 798 MB	P4 2.4 GHz 798 MB	P4 2.4 GHz 798 MB	P4 2.4 GHz 798 MB	P4 2.4 GHz 798 MB

Table 1.2 Simulation condition(cross-sectional channel with microstructures)

CASE	5	6	7	2-D
Length(μ m)	2	2	2	2
Height(μ m)	0.4	0.4	0.4	0.4
Width(μ m)	0.2	0.6	1	
Block Height(μ m)	0.2			
P_{in} (atm)	0.73			
P_{in}/P_e	2.5			
T_g (K)	300			
T_w (K)	323			
T_{block} (K)	523			
Number density	1.79×10^{25}			
Initial number of particles per cell	20			
Number of cells	100x10x20	100x30x20	100x50x20	100x20
CPU time	63 hr	96 hr	134 hr	16 hr
Computer rank equipment	P4 CPU 2.4 GHz 768 MB RAM	P4 CPU 3.0 GHz 1 GB RAM	P 4 CPU 3.0 GHz 2 GB RAM	Core(TM) 2 CPU 1.86 GHz 2GB RAM

u_s slip velocity, m/s
u_w wall velocity, m/s
u_g the gas velocity on a wall, m/s
x, y, z Cartesian axis in physical space
Δt time step, s
λ mean free path, m
ρ density, kg/m^3

Superscripts and Subscripts

e denotes the exit boundary
in denotes the entrance boundary
inc, ref denote the values before and after the molecule impacts the wall, respectively
j the number of cell
k denotes the computed quantities at the *k*th time step
rot associated with the rotational modes
tr associated with the translational modes

REFERENCES

[1] Ho, C. M., and Tai, Y. C., "Micro-Electro-Mechanical-Systems (MEMS) and Fluid Flows," *Annual Review of Fluid Mechanics*, Vol. 30, 1998, pp. 579-612.

Table 1.3 Simulation condition(backward-facing step)

CASE	8	9	10	2-D
Length(μ m)	2	2	2	2
Height(μ m)	0.4	0.4	0.4	0.4
Width(μ m)	0.2	0.6	1	
Step Height (μ m)	0.2			
P_{in} (atm)	0.1			
P_{in}/P_e	2.0			
T_g (K)	300			
T_w (K)	323			
T_{step} (K)	323			
Number density	2.446×10^{24}			
Initial number of particles per cell	20			
Number of cells	60x6x12	60x18x12	60x30x12	60x12
CPU time	4 hr	38 hr	48 hr	5 hr
Computer rank equipment	Core(TM) 2 CPU 1.86 GHz 2GB RAM	P 4 CPU 2.8 GHz 1GB RAM	P 4 CPU 3.0 GHz 2GB RAM	P 4 CPU 3.0 GHz 2GB RAM

Table 2 The approaching level of the 3-D cases to the corresponding 2-D case

	centerline velocity (%) (ratio to 2-D case)	centerline temperature (K) (difference to 2-D case)		
3-D straight rectangular cross-sectional channel				
case 1 (D/H=1)	65%	less than 4K		
case 2 (D/H=1.5)	84%	less than 2K		
case 3 (D/H=3)	99.99%	less than 1K		
case 4 (D/H=5)	99.99%	less than 1K		
3-D straight rectangular cross-sectional channel with microstructures				
		Temperature difference to 2-D case		
		Temperature ratio to 2-D case		
case 5 (D/H=1)	78%	375K	346K	373K
		95%	94%	95%
case 6 (D/H=3)	97%	390K	364K	389K
		99.4%	98.9%	99.4%
case 7 (D/H=5)	97.8%	392K	367K	390K
		99.9%	99.7%	99.7%
3-D straight rectangular cross-sectional channel with a backward-facing step				
case 8 (D/H=1)	67%	less than 1K		
case 9 (D/H=3)	92%	less than 1K		
case 10 (D/H=5)	97%	less than 1K		

[2] Lyshevski, S. E., MEMS and NEMS: Systems, Devices and Structures, CRC Press, 2002.
[3] Karniadakis, G. E., Beskok, A., and Alura, N., *Microflows and Nanoflows: Fundamentals and Simulation, Springer, 2005.*
[4] Bird, G. A., *Molecular gas dynamics and the direct simulation of gas flow*, Oxford University Press 1994.
[5] Hong, Z. C., Zhen C. E., and Yang, C. Y., "A Pdf Description of Momentum Fluctuation Correlations of a Rarefied Free Shear Layer," *Journal of Mechanics*, Vol. 22, 2006, pp. 85-92.

[6] Piekos, E. S., and Breuer, K. S., "Numerical Modeling of Micro-Channel Devices Using the Direct Simulation Monte Carlo Method," *Journal of Fluid Engineering*, Vol. 118, 1996, pp. 464-469.

[7] Oh, C. K., Oran, E. S., and Sincovits, R. S., "Computations of High-Speed, High-Knudsen Number Micro-Channel Flows," *Journal of Thermophysics and Heat Transfer*, Vol. 11, 1997, pp. 497-505.

[8] Mavriplis, C., Ahn, J. C., and Goulard, R., "Heat Transfer and Flowfields in Short Microchannels Using Direct Simulation Monte Carlo," *Journal of Thermophysics and Heat Transfer*, Vol. 11, 1997, pp. 489-496.

[9] Liou, W. W. and Fang, Y., "Heat Transfer in Microchannel Devices Using DSMC," *Journal of Microelectromechanical System*, Vol. 10, 2001, pp. 274-279.

[10] Le, M. and Hassan, I., "Simulation of Heat Transfer in High Speed Microflows," *Applied Thermal Engineering*, Vol. 26, 2006, pp. 2035-2044.

[11] Le, M., Hassan, I., and Esmail, N., "The Effects of Outlet Boundary Conditions on Simulating Supersonic Microchannel Flows Using DSMC," *Applied Thermal Engineering*, Vol. 27, 2007, pp. 21-30.

[12] Muntz, E. P., "Rarefied Gas Dynamics," *Annual Review of Fluid Mechanics*, Vol. 21, 1989, pp. 387-417.

[13] Oran, E. S., Oh, C. K., and Cybyk, B. Z., "Direct simulation Monte Carlo: recent advances and applications," *Annual Review of Fluid Mechanics*, Vol. 30, 1998, pp. 403-441.

[14] Nance, R. P., Hash, D. B., and Hassan, H. A., "Role of Boundary Conditions in Monte Carlo Simulation of MEMS Devices," *Journal of Thermophysics and Heat Transfer*, Vol. 12, 1998, pp. 447-449.

[15] Fan, J., and Shen, C., "Statistical Simulation of Low-speed Rarefied Gas Flows," *Journal of computational physics*, Vol. 167, 2001, pp. 393-412.

[16] Cai, C., Boyd, I. D., and Fan, J., "Direct Simulation Methods for Low-speed Microchannel Flows," *Journal of Thermophysics and Heat Transfer*, Vol. 14, 2000, pp. 368-378.

[17] Sun, H. and Faghri, M., "Effects of Rarefaction and Compressibility of Gaseous Flow in Microchannel Using DSMC," *Numerical Heat Transfer, Part A*, Vol. 38, 2000, pp. 153-168.

[18] Wu, J. S., Lee, F., and Wong, S. C., "Pressure Boundary Treatment in Micromechanical Devices Using the Direct Simulation Monte Carlo Method," *JSME International Journal*, Vol. 44, 2001, pp. 439-450.

[19] Liou, W. W. and Fang, Y., "Implicit Boundary Conditions for Direct Simulation Monte Carlo Method in MEMS Flows Predictions," *Computer Modeling in Engineering & Science*, Vol. 1, 2000, pp. 119-128.

[20] Fang, Y. and Liou, W. W., "Computations of the Flow and Heat Transfer in Microdevices Using DSMC with Implicit Boundary Conditions," *Journal of Heat Transfer Transactions of ASME*, Vol. 124, 2002, pp. 338-345.

[21] Sun, H. and Faghri, M., "Effects of Surface Roughness on Nitrogen Flow in a Microchannel Using the Direct Simulation Monte Carlo Method," *Numer. Heat Transfer, Part A*, Vol. 43, 2003, pp. 1-8.

[22] Wang, M. and Li, Z., "Simulations for Gas Flows in Microgeometries Using the Direct Simulation Monte Carlo Method," *International Journal of Heat and Fluid Flow*, Vol. 25, 2004, pp. 975-985.

[23] Wang, M. and Li, Z., "Three-Dimensional Effect of Gas Flow in Micro-Channels," *Journal of Engineering Thermophysics*, Vol. 25, pp. 840-842.

[24] Zhen, C. E., Hong, Z. C., Lin, Y. J., and Hong, N. T., "Comparison of 3-D and 2-D DSMC Heat Transfer Calculations of Low-Speed Short Microchannel Flows," *Numerical Heat Transfer*, Part A, Vol. 55, 2007, pp. 239-250.

[25] Hong, Zuu-Chang, Zhen, Chaw-En, and Yang, Chien-Yuh, 2008/08, "Fluid Dynamics and Heat Transfer Analysis of Three Dimensional Microchannel Flows With Microstructures," *Numerical Heat Transfer Part A, An International Journal of Computation and Methodology*, Vol. 54, No. 3, pp. 293-314.

[26] Xue, H., Xu, B., Wei Y.,and Wu, J., "Unique Behaviors of a Backward-Facing Step Flow at Microscale," *Numerical Heat Transfer, Part A*, Vol. 47, 2005, pp. 251-268.

[27] Wang, M. and Li, Z., "Gas Mixing in Microchannels Using the Direct Simulation Monte Carlo Method," *International Journal of Heat and Mass Transfer*, Vol. 49, 2006, pp. 1696-1702.

[28] Borgnakke, C., and Larsen, P. S., "Statistical Collision Model for Monte Carlo Simulation of Polyatomic Gas Mixture," *Journal of Computational Physics*, Vol. 18, 1975, pp. 405-420.